Role of SST over the Indian Ocean in Influencing the Intraseasonal Variability of the Indian Summer Monsoon

Mathew ROXY

Graduate School of Environmental Earth Science, Hokkaido University, Sapporo, Japan

and

Youichi TANIMOTO

Faculty of Environmental Earth Science, Hokkaido University, Sapporo, Japan

(Manuscript received 28 September 2006, in final form 24 January 2007)

Abstract

Intraseasonal variability (10–60 days) of sea surface temperature (SST) over the north Indian Ocean and its influence on regional precipitation variability over the Indian subcontinent are examined. SST, cloud liquid water and precipitation over the Indian Ocean of the Tropical Rainfall Measuring Mission (TRMM), precipitation of Climate Prediction Center Merged Analysis of Precipitation (CMAP), and low-level atmospheric parameters of National Center for Environmental Prediction (NCEP) II reanalysis are utilized for this study. Western Ghats (WG) in the southwest and the Ganges-Mahanadi Basin (GB) in the northeast of the Indian subcontinent are observed to be the regions of maximum precipitation with large standard deviations of the intraseasonal variability. Active (break) phases of precipitation occur in these regions by the northward propagation of positive (negative) precipitation anomalies over the Arabian Sea and the Bay of Bengal. Latitude-time plots during the active phase of the WG region shows that the positive SST anomalies over the Arabian Sea formed by suppressed surface latent heat flux and increased downward shortwave radiation flux lead the positive precipitation anomalies. Surface air temperature anomalies follow the SST anomalies and then destabilize the lower atmosphere between 1000 hPa and 700 hPa. These results indicate that, in the northward propagating dynamical surface convergence, underlying SST anomalies tend to form a favorable condition for convective activity and may sustain enhanced precipitation over the convergence region. This results in enhanced precipitation anomalies over the WG region that move further northeastward and merge with the northward propagating precipitation anomalies from the Bay of Bengal, enhancing the active phase of the GB region.

1. Introduction

Lying on both sides of the Indian subcontinent, air sea interaction over the Arabian Sea and the Bay of Bengal are found to influence precipitation variability associated with Indian summer monsoon. The Arabian Sea is a principal source of moisture fluxes across the west coast of India, resulting in periods of heavy orographically forced rainfall over the Western Ghats (WG; Saha and Bavadekar 1977; Rakhecha and Pisharoty 1996). Rakhecha and Pisharoty (1996) found that rainfall over the

Corresponding author: Mathew Roxy, Division of Ocean and Atmospheric Sciences, Graduate School of Environmental Earth Science, Hokkaido University, Sapporo, 060-0810, Japan.
E-mail: rocksea@ees.hokudai.ac.jp

Ganges-Mahanadi River Basins (GB) is associated with tropical depressions formed over the Bay of Bengal, with an effect principally limited to the GB region. Vecchi and Harrison (2004) examined the role of SST anomalies in the northern Indian Ocean in the interannual variability of precipitation in the WG and GB regions, where summer monsoon rainfall shows local maximum in the seasonal mean and its interannual variability. For the WG region, they found a strong positive correlation with SST anomalies in the Arabian Sea at the onset of summer monsoon. Meanwhile, they found no correlations between precipitation anomalies in the GB region and SST anomalies in the Bay of Bengal. They suggest that interannual SST variations in the Bay of Bengal are poorly represented in the SST product of National Centers for Environmental Prediction (NCEP).

Intraseasonal variability of the Indian summer monsoon, delineated by active periods of heavy rainfall interrupted by break periods of deficient, significantly modulates the seasonal mean monsoon fields (Krishnamurthy and Shukla 2000; Goswami and Ajayamohan 2001). This active-break cycle of the Indian summer monsoon is associated with the northward propagation of clouds and convection from the equatorial region to around 30°N over the South Asian monsoon region, at a phase speed of about 1° latitude per day (Yasunari 1979, 1980; Sikka and Gadgil 1980; Gadgil and Asha 1992; Ramesh Kumar et al. 2005). There have been many attempts to develop a theoretical framework of atmospheric dynamics in the northward propagation of the cloud bands on this time scale (Murakami 1984; Jiang et al. 2004; Yokoi and Satomura 2006).

Kemball-Cook and Wang (2001) examined the influence of latent heat flux on the northward migration of outgoing longwave radiation (OLR) anomalies over the Indian Ocean. They suggest that the moisture flux from the ocean to the atmosphere indicated by negative latent heat flux anomalies favors convection by building up moist static energy. However, since their study is based on convective maximum over the equatorial Indian Ocean, the resultant composite signals weaken towards higher latitudes, and hence may not be effective in explaining the processes involving the regional precipitation over the Indian subcontinent. Hence a study focusing on the regional precipitation maximums over the Indian subcontinent and the role of SST on it is sought here. Also, there is a meridional variation of the mean winds from the equator to the north Indian Ocean. Contribution of the zonal wind anomalies to the mean wind speed and the resultant latent heat fluxes should be carefully treated in the analysis.

Vecchi and Harrison (2002) examined intraseasonal variability of outgoing longwave radiation with respect to SST anomalies over the Bay of Bengal. They pointed out that positive (negative) SST anomalies on the intraseasonal scale in the Bay of Bengal exhibit a strong statistical relation with the active (break) periods. Much work on Indian monsoon precipitation has focused on large-scale indicators of precipitation variability, often the total over India, known as All India Rainfall index (AIR, Vecchi and Harrison 2004). Because of the two oceans lying on both sides and orographic features of the Indian subcontinent, the intraseasonal precipitation variability may have regional characteristics along the east and west coast. In the present study, we take into account the regional characteristics of intraseasonal precipitation variability, instead of using the AIR index. This study examines the role of intraseasonal SST anomalies over the Arabian Sea and the Bay of Bengal separately, with respect to regional precipitation variability on the intraseasonal scale. Our analysis on intraseasonal scale is possible due to recent availability of high-quality satellite data.

The rest of paper is organized as follows. In Section 2 we describe datasets and data processing methods used for this study. In Section 3 we explore the regional structure of intraseasonal precipitation variability over the Indian subcontinent. Our focus is the SST variability over the Arabian Sea and the Bay of Bengal, and its influence on the regional precipitation variability over the Indian subcontinent. Section 4 gives concluding remarks and discussion.

2. Data and analysis methods

Until recently, comprehension of observed SST in the north Indian Ocean during the southwest monsoon season has been limited due to sparse ship and buoy sampling of SST (Harrison and Larkin 1996) and heavy cloudi-

ness associated with the monsoon seriously restricting the number of satellite infrared observations. However, since December 1997, Tropical Rain Measuring Mission (TRMM) Microwave Imager (TMI) has provided a novel view of tropical SST variability, unaffected by clouds, aerosols, and atmospheric water vapor (Wentz et al. 2000). Because of its frequent-repeat, non-sun-synchronous orbit, the TMI SST dataset provides uninterrupted pictures of the Indian Ocean SST under active atmospheric convection, which is useful for analysis of intraseasonal SST variability (Senan et al. 2001).

The 3-day running mean SST and cloud liquid water based on TMI on 0.25° grid is used in this study. We used the pentad precipitation based on the Climate Prediction Center Merged Analysis of Precipitation (CMAP), available on 2.5° grid (Xie and Arkin 1996, 1997). To have higher resolution data of precipitation, 3-day running mean TMI precipitation data on 0.25° grid is also utilized over the ocean. The daily 2.5° gridded surface winds, surface latent heat flux (SLHF), downward shortwave radiation flux (DSWRF), and surface air temperature (SAT) based on NCEP Reanalysis II (NCEP II) are also used. Equivalent potential temperature (θ_e) is calculated based on air temperature and specific humidity of NCEP II. The unstable condition of the lower atmosphere is estimated as a difference in θ_e between 1000 hPa and 700 hPa,

$$\Delta\theta_e = \theta_{e1000} - \theta_{e700}$$

where θ_{e1000} and θ_{e700} are θ_e at 1000 hPa and 700 hPa, respectively.

Data of SST, cloud liquid water, and precipitation between June 1 and Sept 30 (summer monsoon) from 1998 to 2002 are interpolated to daily for compatibility among variables. Anomalies are obtained by removing the seasonal means for each of individual years and then those anomalies are band pass filtered using a boxcar filter to retain intraseasonal variability between 10–60 days. These intraseasonally filtered anomalies are used in our study.

3. Results

3.1 Intraseasonal precipitation variability over the Indian subcontinent

To analyze the regional characteristics of precipitation over the Indian subcontinent on intraseasonal scales, we plot the summertime standard deviations (June to September) of intraseasonal variability in Fig. 1. Large standard deviations of the intraseasonal variability emerge over two regions in the Indian subcontinent, over the WG (72.5–77.5°E, 7.5–20°N) and GB (77.5–87.5°E, 20–27.5°N) regions. The time series of the intraseasonal variability averaged over these two regions (Fig. 2) show larger amplitudes in the WG region than in the GB region and are not simultaneously correlated to each other (correlation of 0.03). However, later in this study, it is shown that precipitation anomalies at these two regions are having a lag-lead correlation. Since there is no simultaneous correlation but a lag-lead correlation between the two regions of precipitation, and since the two oceans lying on either side could have different influence on them, examining the intraseasonal variability of precipitation in each region is essential instead of a use of the AIR index.

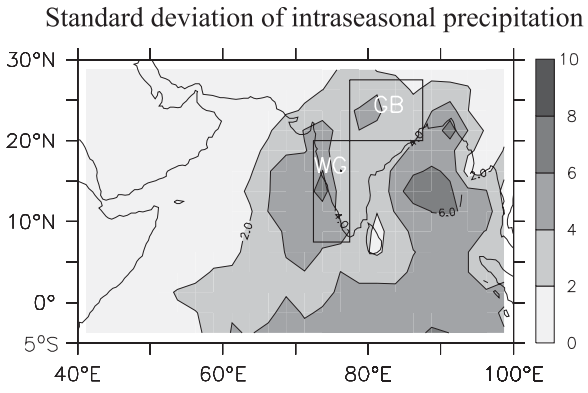

Fig. 1. Standard deviation of intraseasonal variability of precipitation (unit: mm day^{-1}) for JJAS (1998–2002). Shading convention is represented on the side of the panel. Contour lines (interval: 2 mm day^{-1}) of precipitation are superimposed. The southwest (northeast) inset rectangle represents the WG (GB) region.

3.2 WG region

To examine temporal evolution of the intraseasonal precipitation variability over the WG region, we define the WG active phase as the days when the intraseasonal precipitation anomalies in that region (Fig. 2, black curve)

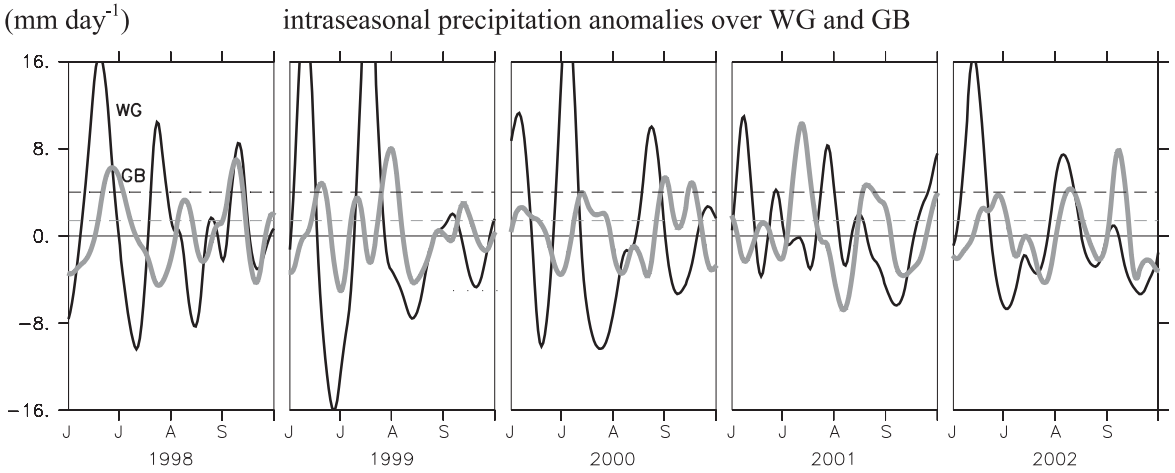

Fig. 2. Intraseasonal time series of precipitation anomalies (unit: mm day^{-1}) averaged over the WG (black curve) and the GB (gray curve) regions. An active phase for each of the regions is defined as when the intraseasonal precipitation is above 0.6 standard deviation.

exceeds a threshold value of 0.6 standard deviation (4 mm day^{-1}), representing strong anomalous precipitation. Most of the WG active phases have 5–7 days duration. Thirteen (13) events of the WG active phases are identified during 1998–2002. We also define the WG pre-active (post-active) phase as 10 days before (after) each day of the active phase because this period (20 days) roughly represents half of the active-break cycle. Figure 3 shows composite maps of the intraseasonal precipitation, surface wind, and SST anomalies during these three phases. During the WG pre-active phase (Fig. 3a), weakly positive anomalies ($\sim$1 mm day^{-1}) of precipitation are found in the southeastern part of the Arabian Sea and in the southwestern part of the Bay of Bengal. These precipitation anomalies propagate northward and begin to intensify (5$\sim$7 mm day^{-1}) during the WG active phase, eventually triggering enhanced precipitation near west coast of the WG region. Another local precipitation maximum with less intensity ($\sim$5 mm day^{-1}) is also located over the Bay of Bengal during the active phase. These anomalies propagate further northward during the WG post-active phase, and then weakened anomalies ($\sim$1 mm day^{-1}) locate over the GB region (Fig. 3c).

In the region of the enhanced precipitation anomalies, an anomalous convergence of surface winds is observed (Fig. 3a). The intraseasonal surface wind anomalies over the south Arabian Sea during the pre-active phase are northeasterlies ($\sim$1 ms^{-1}), which results in reduced wind speed because the seasonal mean winds are southwesterly. This weak wind speed causes the positive SST anomalies ($\sim$0.3°C) over the same region by the reduced heat release from the ocean. This is followed by an abrupt shift to anomalous southwesterlies ($\sim$1 ms^{-1}) in the southern part of the Arabian Sea during the active phase, forming a meridional gradient with negative (positive) SST anomalies in the south (north) of the Arabian Sea (Fig. 3b). The local SST maximum leads relative to the northward-migrating enhanced precipitation, indicating that a warm ocean surface induced by weak wind speed may contribute to a favorable condition of the convective activity as in the tropics.

To examine the phase relationship among the intraseasonal precipitation and SST anomalies over Arabian Sea, we made hovmoller plots of daily composite variables averaged over 60–70°E (left inset rectangle in Fig. 3c), from the WG pre-active to the WG post-active phase. Coherent northward migrations (0.9° per day) of the anomalies over the Arabian Sea are observed (Fig. 4a) where positive SST anomalies (0.2–0.4°C) lead by 1/4 of the cycle the positive precipitation anomalies (4–6 mm day^{-1}). Though less intense, the negative

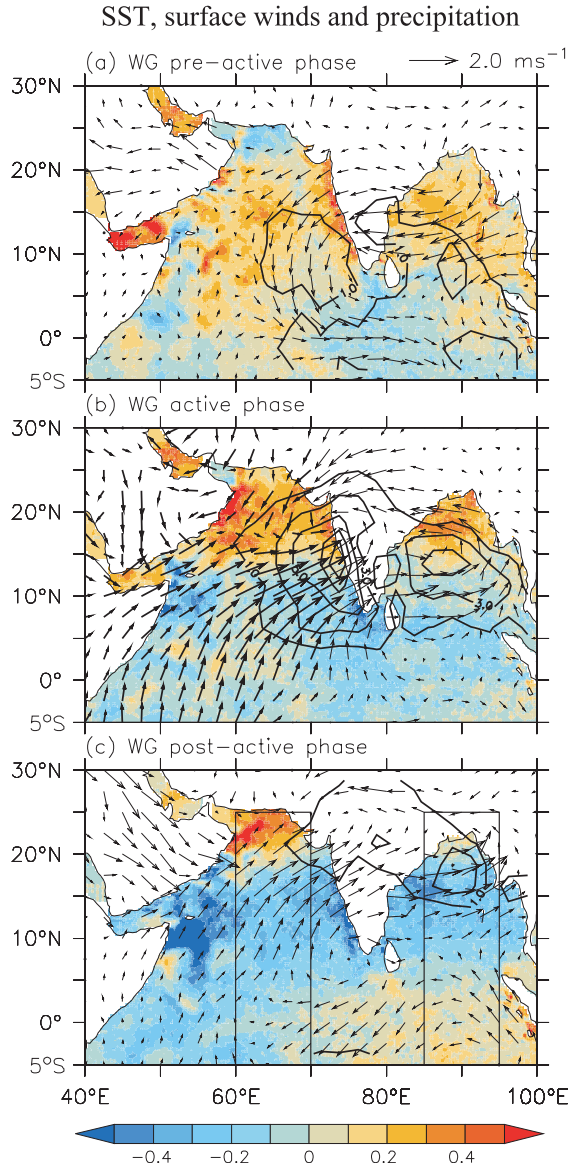

Fig. 3. Composites of intraseasonal SST (colors; unit: °C), surface winds (arrows) and precipitation (contour lines; unit: mm day^{-1}) anomalies during the WG active phase. The inset rectangle in Fig. 3c indicates the domains for the hovmoller plots of the Arabian Sea (60–70°E, Fig. 4) and the Bay of Bengal (85–95°E, Fig. 7). Contour lines of 1.0, 3.0, 5.0, and 7.0 mm day^{-1} are plotted. Scaling of arrows (unit: ms^{-1}) is given on top of the figure. Coloring convention is represented at the bottom of the figure.

SST and precipitation anomalies follow the positive anomalies, making an intraseasonal cycle of 40∼50 days. For simplicity, we will focus on the active phase with the positive precipitation and SST anomalies.

For a further evaluation of the role of SST anomalies in influencing the intraseasonal precipitation variability, the same hovmoller plots are made using zonal surface winds, SLHF, DSWRF, SAT, $\Delta\theta_e$, and cloud liquid water anomalies (Fig. 5). All panels in Fig. 5 depict a coherent northward propagation of the intraseasonal anomalies from 5°N to 20°N. Coherent northward propagation was not observed in the meridional wind anomalies (not shown). Figures 5a and 5b show that anomalous easterly surface winds that oppose the climatological southwesterlies induce reduced evaporative cooling as shown by positive SLHF anomalies (30 Wm^{-2}, downward positive). Positive DSWRF anomalies (Fig. 5c, 30 Wm^{-2}) appear at the same time, with intensity comparable to the SLHF anomalies, warming the ocean surface. The SLHF anomalies are prominent north of 15°N, while the DSWRF anomalies are prominent around 15°N. Positive sensible heat net flux and net longwave radiation flux anomalies were also observed to be in phase with the other surface heat fluxes, but they are too small in comparison and hence not shown here. This suggests that SLHF and DSWRF anomalies contribute to the evolution of positive SST anomalies (∼0.3°C, contours in Fig. 5) with the SLHF anomalies playing significant role over the northern Arabian Sea. The extent to which the surface heat flux anomalies can account for the observed intraseasonal variations of SST were examined using the SST tendency equation

$$\frac{\partial T_s}{\partial t} = \frac{F_{tot}}{\rho c_p h}$$

where T_s is the SST, F_{tot} is the total heat flux, ϱ is density of water, c_p is the specific heat of water at constant pressure, and h is the depth of the mixed layer averaged as 40 m for the Indian Ocean during June to September (Kara et al. 2003). The observed SST tendency varied coherently with those derived from the surface heat fluxes, both in amplitude and phase (Figs. 5d and 5e), supporting the aforementioned relationship. For instance, with an F_{tot} of 50 Wm^{-2},

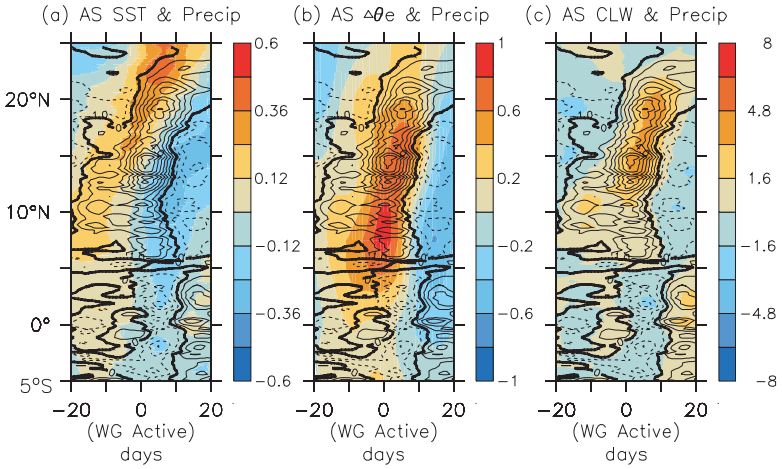

Fig. 4. Hovmoller plots of intraseasonal anomalies of (a) SST (colors; unit: °C), (b) $\Delta\theta_e$ (colors; unit: K) and (c) cloud liquid water (colors; unit: mm) over the Arabian Sea during the WG active phase. Contour lines of TMI precipitation anomalies (interval: 1 mm day^{-1}) are superimposed, with negative values dashed. Coloring convention is represented at the side of each panel.

h of 40 m, and standard values of ϱ and c_p, the heat flux forcing estimated is in the order of 0.025°C day^{-1}. This is comparable to the SST variability of 0.02°C day^{-1}, estimated for an SST change of 0.8°C in 40 days.

The positive SST anomalies are followed by comparable magnitude of positive SAT anomalies (Fig. 5f), indicating ocean-to-atmosphere effect near the sea surface. These positive SAT anomalies induce the positive anomalies in $\Delta\theta_e$ (0.6°C) over the same region (Fig. 5g), a condition favoring convective activity. Even though positive anomalous $\Delta\theta_e$ maximum appears to be collocated with SLHF anomalies, the phase change of positive $\Delta\theta_e$ anomalies leads the phase change of negative SLHF anomalies. This indicates that the negative SLHF anomalies cannot account for the observed phase change in the $\Delta\theta_e$ anomalies, suggesting the effect of SAT anomalies on the $\Delta\theta_e$ anomalies. Indeed, θ_{e1000} anomalies were observed to be nearly equal to SAT anomalies. The positive $\Delta\theta_e$ anomalies render adequate unstable condition before the active phase. The destabilization of the lower atmosphere may provide the uplift of the moisture content from the lower atmosphere and the consequent condensation resulting in positive cloud liquid water anomalies (~0.04 mm, Fig. 5h), giving rise to enhanced precipitation. Indeed, positive precipitation anomalies coincide with unstable condition in the lower atmosphere (Fig. 4b) and abundant cloud liquid water (Fig. 4c). These findings suggest an SST effect on the convective clouds through changes in the vertical structures of the lower-tropospheric temperature and moisture content. The suggested SST effect appears to work effectively over the off-equatorial regions in the Arabian Sea, in the 10 to 25°N band, where the SST anomalies are significant.

3.3 *GB region*

In Fig. 3, the composite precipitation anomalies after the WG active phase further propagate northward and are eventually displaced into over the GB region. With the same manner of the WG active phase, we define the GB active phase based on the gray curve in Fig. 2, when the threshold value exceeds 0.6 standard deviation (1.4 mm day^{-1}). Sixteen (16) events of the GB active phases are identified. As for the WG active phase, we also define the GB pre-active and post-active phases. Figure 6 shows composite maps of the intraseasonal precipitation, surface wind, and SST anomalies during these three phases. During the GB pre-active phase (Fig. 6a), two local maxima of precipitation anomalies locate along WG and in the Bay of Bengal. In a broad sense, these two maxima are also present during the WG active phase

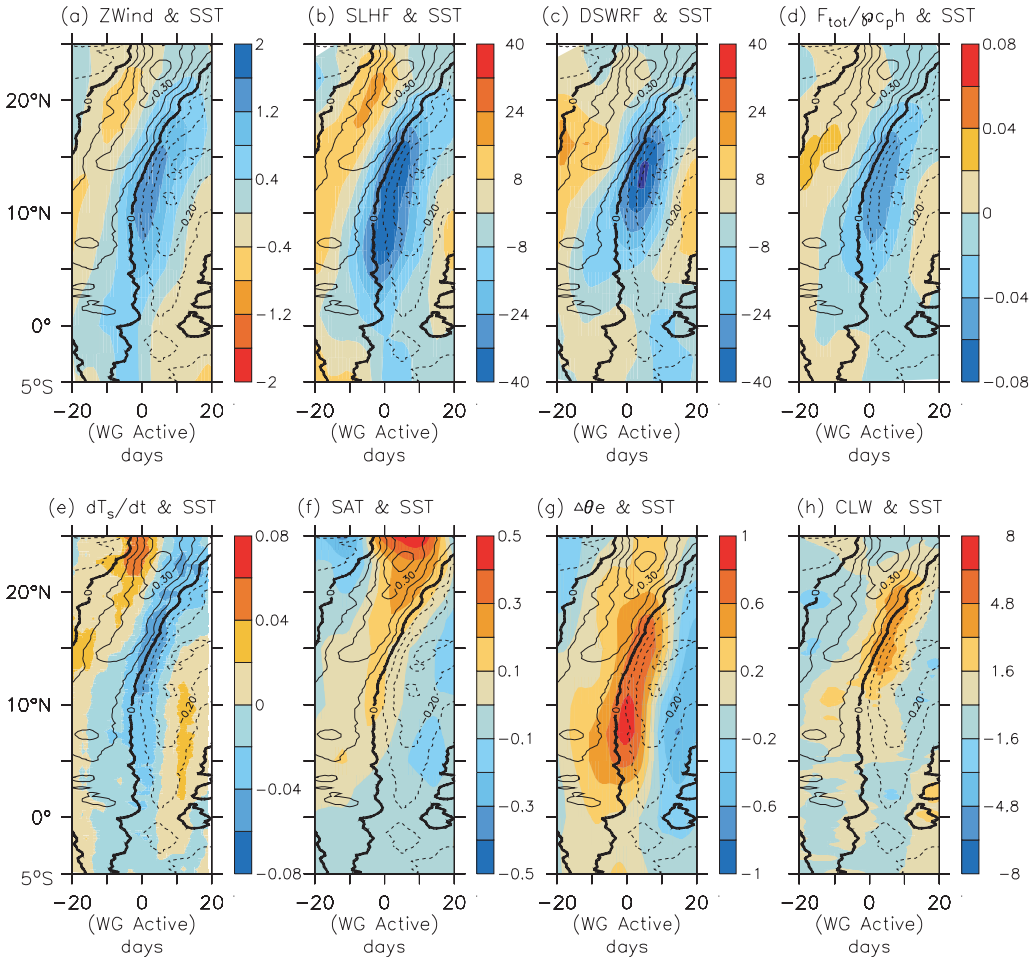

Fig. 5. Hovmoller plots of intraseasonal anomalies of (a) surface zonal wind (colors; unit: ms^{-1}), (b) surface latent heat flux (colors; unit: Wm^{-2}), (c) downward shortwave radiation flux (colors; unit: Wm^{-2}), (d) surface heat flux forcing (colors; unit: °C day^{-1}), (e) SST tendency (colors; unit: °C day^{-1}), (f) surface air temperature (colors; unit: °C), (g) $\Delta\theta_e$ (colors; unit: K) and (h) cloud liquid water (colors; unit: mm) over the Arabian Sea during the WG active phase. Contour lines of SST anomalies (interval: 0.1°C) shown in Fig. 4a are superimposed, with negative values dashed. Coloring convention is represented at the side of each panel.

(Fig. 3b). These anomalies are observed to move northward and eventually merged at around 22°N, 80°E during the GB active phase (Fig. 6b). Though less intense, the merged precipitation anomalies are present during the WG post-active phase (Fig. 3c). These results show that the GB active phase tends to occur 5–10 days after the WG active phase. Indeed, the highest lag correlation coefficient is 0.44 when the WG time series leads the GB time series by 10 days (Fig. 2).

Factors other than the further northeastward propagation of precipitation from the WG region may also contribute to the GB active phase, such as SST anomalies over the Bay of Bengal. Local maximum of SST anomalies in the Bay of Bengal is northward displaced relative to the enhanced precipitation in Figs. 6a and 6b. A hovmoller plot of composite SST and precipitation anomalies averaged over the Bay of Bengal (85–95°E; right inset rectangle in Fig. 3c) during the GB active phase (Fig. 7) shows a similar ocean-to-atmosphere effect over the off-equatorial regions of the Bay of

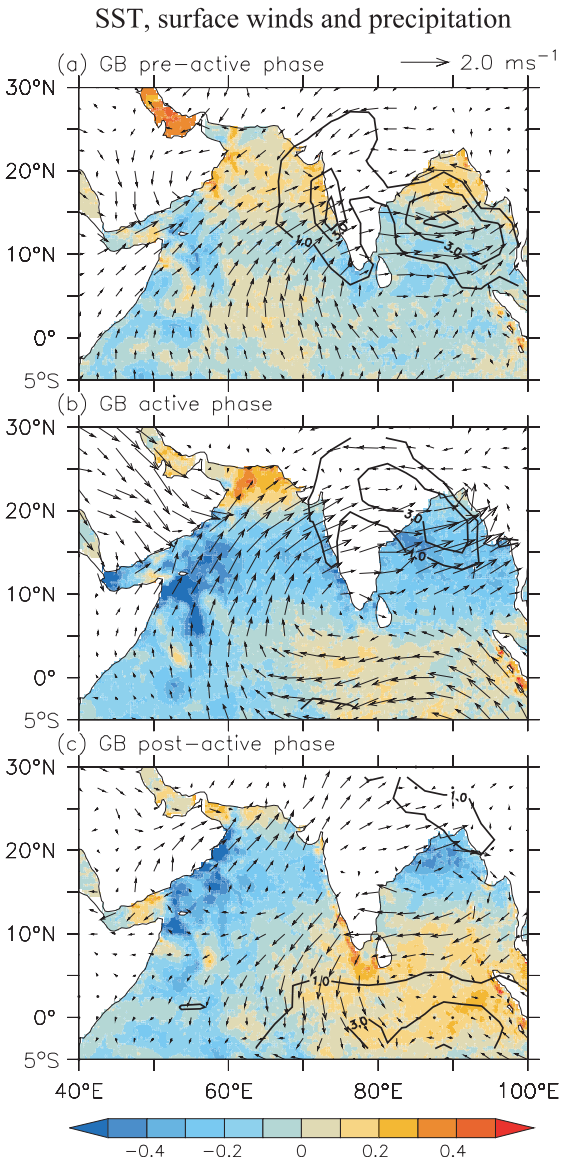

Fig. 6. Same as in Fig. 3, but for the GB active phase.

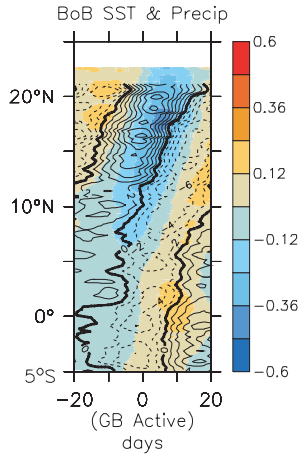

Fig. 7. Same as in Fig. 4a, but for over the Bay of Bengal during the GB active phase.

Bengal, in a similar manner as over the Arabian Sea (Fig. 4). Though the SST anomalies are weak (~0.2°C in 15–25°N), compared to those observed over the Arabian Sea, they are followed by enhanced precipitation anomalies (~5 mm day^{-1}). This anomalous precipitation moves further northward, merges with the precipitation anomalies from the WG region (Fig. 6b), and provides in-land anomalous precipitation at 25°N during the GB active phase. The result implies that ocean-to-atmosphere effect over the Arabian Sea and the Bay of Bengal influences the GB active phase.

4. Concluding remarks and discussion

Using observed SST, precipitation, surface wind, SLHF, DSWRF, SAT, equivalent potential temperature, and cloud liquid water, we have analyzed the relationship between the SST over the Indian Ocean and the Indian summer monsoon on intraseasonal timescales. The intraseasonal precipitation anomalies over the WG and GB regions are simultaneously uncorrelated to each other, with the former influenced by the ocean-to-atmosphere effect over the Arabian Sea and the latter by both the Arabian Sea and Bay of Bengal. This suggests that intraseasonal precipitation variability over each region should be examined separately for studies involving the variability over the Indian subcontinent as a whole. Over the Arabian Sea, positive SLHF induced by reduced wind and positive DSWRF anomalies are observed to contribute to the evolution of positive SST anomalies. These northward propagating (at 0.9°/day) positive SST anomalies are found to lead the positive SAT anomalies, indicating ocean-to-atmosphere effect near the sea surface. The positive SST anomalies are followed by the positive $\Delta\theta_e$ anomalies, suggesting the active role of SST anomalies in inducing unstable conditions over the lower atmosphere, which

results in enhanced precipitation over the Arabian Sea and the WG region. The positive precipitation anomalies during the WG active phase propagate further northward, contributing to the GB active phase, 10 days after the WG active phase. Also, a similar ocean-to-atmosphere effect over the Bay of Bengal may contribute to the GB active phase. A quantitative estimation of how much the Arabian Sea and the Bay of Bengal contribute to the GB active phase is left for future research.

Prior to the WG active phase, an anomalous surface convergence associated with northeasterlies (southwesterlies) of the surface winds in the northern (southern) part of the Arabian Sea enhances convective precipitation. According to Jiang et al. (2004), the easterly vertical shear (the upward increase of easterlies) over the anomalous surface convergence in the lower atmosphere tends to generate anomalous moisture convergence north of the center of precipitation anomalies, leading to the northward shift of the anomalous surface convergence and precipitation. Their study shows that the northward migration of precipitation anomalies is caused by this vertical shear mechanism. Hsu et al. (2004, 2005) suggest that the eastward extension of the northward propagating precipitation anomalies from the Arabian Sea could be driven by the anomalous surface convergence located to the east of the deep convection region, which is in turn induced by the lifting and frictional effects of the geography over the west coast of the Indian subcontinent. Rossby wave response to heating sources over the equatorial Indian Ocean have been linked in remotely enhancing the northward propagating precipitation anomalies (Lawrence and Webster 2002; Annamalai and Sperber 2005). In the present study, it is shown that the underlying positive SST anomalies enhance the northward propagating precipitation anomalies over the Arabian Sea in a thermodynamical way.

Kemball-Cook and Wang (2001) had earlier pointed out that negative SLHF anomalies contribute to enhancing the convective activity through an increase in the moist static energy. In their study, it is given that anomalous easterlies coincide with the development of negative SLHF anomalies, which results in an increase in the moist static energy. Since the climatological zonal winds are westerly at the surface, the anomalous surface easterlies against the mean flow result in positive SLHF anomalies. In that case, the wind induced positive SLHF anomalies cannot directly account for the positive moist static energy anomalies observed in their study. As also shown in the present study, the observed anomalous easterlies induce the positive SLHF anomalies, resulting in positive SST anomalies (Figs. 5a and 5b). These positive SST anomalies play a role in enhancing the positive $\Delta\theta_e$ anomalies of the lower atmosphere (Fig. 5g), resulting in a condition favorable for enhanced precipitation (Figs. 4a and 5h). It is also to be noted that an increase in SST enhances the moisture holding capacity of the lower atmosphere and hence is significant while considering moist static energy.

Thus, the results presented herein suggest that SST anomalies over the north Indian Ocean are significant in locally enhancing the northward propagating precipitation anomalies. The significant lead of positive SST anomalies to the WG and GB active phases provides a useful precursor of the active spells in the Indian summer monsoon.

Acknowledgements

The TRMM data is obtained from Remote Sensing Systems and the NCEP/NCAR Reanalysis data from the NOAA Climate Diagnostics Center. The CMAP data is supplied by the NOAA Climate Diagnostics Center. Insightful comments by the two anonymous reviewers led to substantial improvements in the manuscript. This work was partly supported by Grand-In-Aid for Scientific Research defrayed by the Ministry of Education, Culture, Sports, Science and Technology of Japan (17340137) and the Sumitomo foundation. We gratefully acknowledge financial support from the Center of Excellence, Graduate School of Environmental Earth Science, Hokkaido University.

References

Annamalai, H. and K.R. Sperber, 2005: Regional heat sources and the active and break phases of boreal intraseasonal (30–50 day) variability. *J. Atmos. Sci.*, **62**, 2726–2748.

Gadgil, S. and G. Asha, 1992: Intraseasonal Variation of the Summer Monsoon I: Observational Aspects. *J. Meteor. Soc. Japan*, **70**, 387–397.

Goswami, B.N. and R.S. Ajayamohan, 2001: Intraseasonal oscillations and interannual variability of the Indian summer monsoon. *J. Climate*, **14**, 1180–1198.

Harrison, D.E. and N.K. Larkin, 1996: The COADS sea level pressure signal: A near-global El Niño composite and time series view. 1946–1993. *J. Climate*, **9**, 3025–3055.

Hsu H.-H., C.-H. Weng, and C.-H. Wu, 2004: Contrasting characteristics between the northward and eastward propagation of the intraseasonal oscillation during the boreal summer. *J. Climate*, **17**, 727–743.

Hsu, H.-H. and M.-Y. Lee, 2005: Topographic effects on the eastward propagation and initiation of the Madden-Julian Oscillation. *J. Climate*, **18**, 795–809.

Jiang, X., T. Li, and B. Wang, 2004: Structures and mechanisms of the northward propagating boreal summer intraseasonal oscillation. *J. Climate*, **17**, 1022–1039.

Kemball-Cook, S. and B. Wang, 2001: Equatorial waves and air–sea interaction in the boreal summer intraseasonal oscillation. *J. Climate*, **14**, 2923–2942.

Krishnamurthy, V. and J. Shukla, 2000: Intraseasonal and interannual variability of rainfall over India. *J. Climate*, **13**, 4366–4377.

Murakami, T., T. Nakazawa, and J. He, 1984: On the 40–50 day oscillations during the 1979 Northern Hemisphere summer. I: Phase propagation. *J. Meteor. Soc. Japan*, **62**, 440–468.

Rakhecha, P.R. and P.R. Pisharoty, 1996: Heavy rainfall during monsoon season: Point and spatial distribution. *Curr. Sci*., **71**, 179–186.

Ramesh Kumar, M.R., S.S.C. Shenoi, and J. Schultz, 2005: Impact of convection over the equatorial trough on summer monsoon activity over India. *Int. J. Remote Sens*., **26**, 4747–4762.

Saha, K.R. and S.N. Bavadekar, 1977: Moisture flux across the west coast of India and rainfall during the southwest monsoon. *Quart. J. Roy. Meteor. Soc*., **103**, 370–374.

Senan, R., et al., 2001: Validation of SST and wind speed from TRMM using North Indian Ocean moored buoy observations, Indian Institute of Science, Bangalore, India. 29 pp.

Sikka, D.R. and S. Gadgil, 1980: On the maximum cloud zone and the ITCZ over Indian longitudes during the southwest monsoon. *Mon. Wea. Rev*., **108**, 1840–1853.

Vecchi, G.A. and D.E. Harrison, 2002: Monsoon breaks and subseasonal sea surface temperature variability in the Bay of Bengal. *J. Climate*, **15**, 1485–1493.

Vecchi, G.A. and D.E. Harrison (Eds.), 2004: Interannual Indian rainfall variability and Indian Ocean sea surface temperature anomalies, 247–260, American Geophysical Union, Geophysical Monograph, Washington D.C.

Webster, P.J., et al., 1998: Monsoons: Processes, predictability and the prospects of prediction. *J. Geophys. Res*., **103**, 14451–14510.

Wentz, F., et al., 2000: Satellite measurements of sea surface temperature through clouds. *Science*, **288**, 847–850.

Xie, P. and P.A. Arkin, 1996: Analyses of global monthly precipitation using gauge observations, satellite estimates, and numerical model predictions. *J. Climate*, **9**, 840–858.

Xie, P. and P.A. Arkin, 1997: Global precipitation: a 17-year monthly analysis based on gauge observations, satellite estimates, and numerical model outputs. *Bull. Amer. Meteorol. Soc*., **78**, 2539–2558.

Yasunari, T., 1979: Cloudiness fluctuation associated with the Northern Hemisphere summer monsoon. *J. Meteor. Soc. Japan*, **57**, 227–242.

Yasunari, T., 1980: A quasi-stationary appearance of 30–40 day period in the cloudiness fluctuations during the summer monsoon over India. *J. Meteor. Soc. Japan*, **58**, 225–229.

Yokoi, S. and Satomura, T., 2006: Mechanisms of the northward movement of submonthly scale vortices over the Bay of Bengal during the boreal summer. *Mon. Wea. Rev*., **134**, 2251–2265.